ADVANCED FUNCTIONAL MATERIALS
www.afm-journal.de

Transforming One-Dimensional Nanowalls to Long-Range Ordered Two-Dimensional Nanowaves: Exploiting Buckling Instability and Nanofibers Effect in Holographic Lithography

*Jie Li, Yigil Cho, In-Suk Choi, and Shu Yang**

Two-dimensional nanowaves with long-range order are fabricated by exploiting swelling-induced buckling of one-dimensional (1D) nanowalls with nanofibers formed in-between during holographic lithography of the negative-tone photoresist SU-8. The 1D film goes through a constrained swelling in the development stage, and becomes buckled above the critical threshold. The degree of lateral undulation can be controlled by tuning the pattern aspect ratio (height/width) and exposure dosage. At a high aspect ratio (e.g., 6) and a high exposure dosage, nanofibers (30–50 nm in diameter) are formed between the nanowalls as a result of overlapping of low crosslinking density regions. By comparing experimental results with finite-element analysis, the buckling mechanism is investigated, which confirms that the nanofibers prevent the deformed nanowalls from recovery to their original state, thus, leading to long-range ordered two-dimensional (2D) wavy structures. The film with nanowaves show weaker reflecting color under an ambient light and lower transmittance compared to the straight nanowalls. Using double exposure through a photomask, patterns consisting of both nanowaves and nanowalls for optical display are created.

1. Introduction

Periodically structured materials, whose physical properties are functions of the structural parameters, including shape, geometry, size, orientation and arrangement, are of wide interests for applications, such as controlling the light, sound or heat wave propagation,[1,2] wetting,[3,4] adhesion,[5,6] and cell sensing and proliferation.[7] In many applications, high aspect ratio (AR = height/width) structures are desired. For example, as plasma etching masks, they offer better etching resistance and structure fidelity.[8,9] As grating structures, high AR could lead to new properties, such as blazed transmission gratings via total external reflection on the grating sidewalls for X-rays incident at graze angles.[10] As photonic crystals, high AR structures have higher intensity reflection peak at the photonic stop band.[11]

However, high AR structures are mechanically unstable. When the film is developed in the lithographic process it tends to collapse due to capillary force[12–15] or to be buckled due to anisotropic swelling.[16,17] Specifically, it has been shown that one-dimensional (1D) structures can be laterally buckled into irregular two-dimensional (2D) wavy patterns due to compressive residual stress generated in the film confined on a rigid substrate, for example, by deposition of a thin layer of metal or semiconductor,[18,19] or by swelling.[16] Because the compressive stresses induced by swelling and heating/cooling are isotropic laterally, most of the buckling structures reported in literature are random. It will be intriguing to harness such instability for pattern transformation, specifically, to create highly ordered, high AR 2D wavy patterns by lateral buckling of 1D high AR structures, leading to very different physical properties.

Here, we created highly ordered 2D nanowaves from a commonly used negative-tone photoresist SU-8 during two-beam holographic lithography (HL) by buckling of high AR (up to 6) 1D nanowalls (periodicity of 600 nm). During the development stage, the 1D pattern went through a constrained swelling in the good solvent, leading to the global buckling. The degree of lateral undulation could be controlled by tuning the pattern AR and exposure dosage. Different from literature, the nanowalls in our system were buckled in the same direction with long-range ordering. Between the nanowalls, interconnecting nanofibers (30–50 nm in diameter) were formed between nanowalls when exposed to high dosages. By comparing experimental results with finite-element analysis, we confirmed that nanofibers formed only in the buckled film when the neighboring walls were close enough; they prevented the recovery of the deformed nanowalls to their original state, thus, minimizing random instability after critical point drying. The nanowave structure showed weaker reflecting color under an ambient light and lower transmittance compared to the nanowalls. Using double

J. Li, Dr. Y. Cho, Prof. S. Yang
Department of Materials Science and Engineering
University of Pennsylvania
3231 Walnut Street, Philadelphia, PA 19104
E-mail: shuyang@seas.upenn.edu
Dr. Y. Cho, Dr. I.-S. Choi
High Temperature Energy Materials Research Center
Korea Institute of Science and Technology
L0419, 14–5 Hwarang-ro, Seongbuk-gu, Seoul, 136–791
Republic of Korea

DOI: 10.1002/adfm.201302826

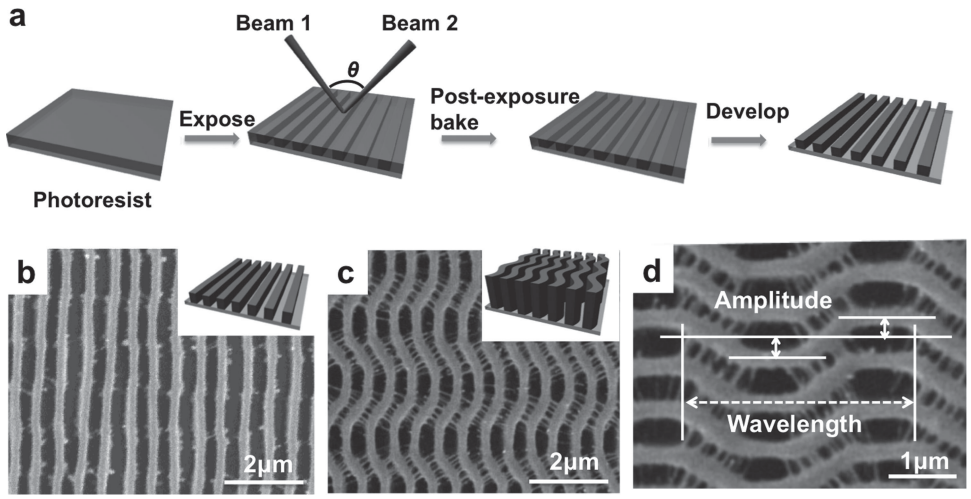

Figure 1. Fabrication of 1D nanowalls and 2D nanowaves via two-beam holographic lithography. a) Schematics of the lithographic process. b,c) Top-view SEM images and schematics of b) 1D nanowalls (width 300 nm, pitch 600 nm, AR ≈ 2) and c) 2D nanowaves (width 300 nm, pitch 600 nm, AR ≈ 6). d) Higher magnification SEM image of (c) with indication of the amplitude and wavelength of the nanowaves. Amplitude is indicated as the distance between center of the original wall to that of the maximum buckled position. Wavelength is the longitudinal periodicity of the nanowaves.

exposure through a photomask, followed by development, we created patterns consisting of both nanowaves and nanowalls for optical display by harnessing the distinct optical properties in the two regions.

2. Results and Discussion

The 1D nanowalls were fabricated by two-beam HL (see experimental section and **Figure 1**a), including photoresist spin-coating, pre-exposure bake, exposure, post-exposure bake (PEB), development, solvent rinsing and critical-point drying (CPD). By recording the interference pattern into a selective photoresist, HL has been used to fabricate 1D, 2D, and 3D periodic structures over a large area.[20,21] The periodicity of the 1D structure could be tuned from a hundred of nanometers to several micrometers using the green laser by varying the angle between two incident laser beams.[22] Here, we kept the periodicity constant at 600 nm and the line width around 300 nm for the interest of grating color in the visible to infrared wavelength. The AR of 1D structure was varied by the concentration of SU-8 solution and spin-coating speed, which determined the film thickness.

SU-8 (Figure S1, Supporting Information), a multifunctional epoxy derivative of a bisphenol-A novalac,[23] was chosen as the model photoresist because of its compatibility with conventional photolithography and HL,[24] and high solubility in many organic solvents, allowing for preparation of thick films with high AR. When SU-8 films of different thickness were exposed to the same HL conditions, followed by development in propylene glycol monomethyl ether acetate (PGMEA) and CPD, different types of nanostructures were observed depending on the AR (see Figure 1). For AR = 2 samples, 1D pattern of straight walls (Figure 1b) were observed as expected from two-beam interference. However, for AR = 6 samples, highly ordered 2D nanowaves were observed (Figure 1c) with wavelength of 3 μm and amplitude of 300 nm (see schematic in Figure 1d).

Buckling of 1D lines to 2D wavy patterns has been reported, typically via thermal or solvent swelling induced stress.[16–19] The 1D lines generally buckle randomly in the xy plane due to isotropic lateral force. In comparison, the nanowaves formed in our system were highly ordered: they all bent in the same direction, which persisted over a large area (5 mm in diameter). A closer look showed that there were many nanofibers formed between the nanowalls in the nanowave samples (e.g., AR = 6, Figure 1d). The role of the fibers will be discussed in detail later.

Swelling-deswelling of SU-8 thin films have been investigated to optimize the processing conditions in photolithography,[25,26] to study pattern transformation in 2D membranes,[27,28] and 3D phononic crsytals,[29] and to enhance grafting of polymer brushes on 2D and 3D structures.[30] Typically in photolithography of 1D structures, pattern collapse of high AR structures is observed due to capillary force during drying. Since we dried the films using CPD, the effect of capillarity should be minimal here. We suspect that the buckling occurred in our 1D structures should be attributed to solvent swelling in the development stage.

Because SU-8 film was confined on a rigid glass substrate, the outer layer would swell more than the layer attached to the substrate, generating an anisotropic osmotic pressure. Meanwhile, the glassy SU-8 was softened by the developer, thus, lowering the buckling threshold. When the AR is large enough, the compressive force generated at the top of the structure could go beyond the buckling threshold, thus, triggering global buckling of the 1D lines. Supporting this, we observed the buckling of 1D structure under the optical microscope from the developed film immersed in the rinsing solvent, isopropanol (IPA) (Figure S2, Supporting Information). We did not directly observe the developed film in PGMEA since it was not compatible with the optical microscope. The extent of buckling and morphology could be controlled by material properties, including crosslinking density and modulus, pattern geometry, and polymer-solvent interaction in a nonlinear manner.

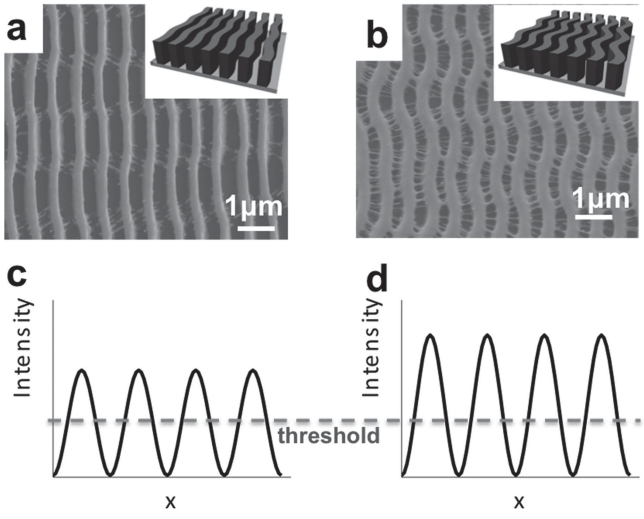

Figure 2. Effect of exposure dosage on the degree of buckling of the 1D nanowalls. a,b) Top-view SEM images and schematics (insets) of nanowaves obtained from HL with exposure time of a) 16 s and b) 17 s, resulting in line width of 250 nm and 350 nm, respectively, and different degree of buckling. The later has significant amount of fibers formed between the walls. c,d) Schematics of two-beam interference intensity profile at different exposure dosages. Regions exposed with intensity higher than the threshold are more crosslinked and remained on the substrate after developing in a good solvent.

The modulus of the as-fabricated SU-8 was measured by AFM nano-indentation, 1.7 GPa, and the swelling ratio in PGMEA was ≈ 1.05–1.1, which agreed well with literature.[25] If keeping AR constant, but exposing the SU-8 film at a higher dosage, more photoacids will be generated, leading to higher crosslinking density and higher filling fraction. Thus, we should expect higher film stiffness, which is less prone to buckling. The effect of exposure dosage is shown in **Figure 2**, where samples had the same film thickness (1 μm) but different exposure time (16 s vs 17 s). Although we did observe increased filling fraction in the film exposed for 17s (Figure 2b) compared to that from 16 s (Figure 2a), the nanowaves were found formed in the 17 s film, contrary to the prediction. Comparing the straight 1D nanowalls and 2D nanowaves, it was clear that the buckled films all had nanofibers (30–50 nm) (see Figures 1, 2); the longer exposure time, the more nanofibers were generated. Nanofiber formation is known to be a byproduct of long exposure during HL.[31] As shown in Figure 2c-d, such effect can be explained by the intensity profiles at different exposure dosage. When the exposure time is increased, interference beam intensity increases. The originally weakly crosslinked regions under shorter exposure time, which would have been removed by developer, now received interference intensity above the critical threshold and become partially crosslinked. Not only the volume-filling fraction is increased but the spacing between neighboring lines becomes smaller due to increase of weakly polymerized regions. It was reported that nanofibers formed and bridged the neighboring nanostructures by networking between the weakly polymerized regions of the nanostructures once the weakly polymerized regions became overlapped withthin an optimized distance.[31] Hence, we speculate that the highly dosaged walls had large enough weakly polymerized regions, which was overlapped during global buckling of the 1D walls. Once the distance of the neighboring walls reaching the threshold, the nanofibers began to form from the walls and finally connected the neighboring walls as shown in the Figure 2b. We also hypothesize that the formation of nanofibers would prevent the buckled SU-8 film from returning to the original straight nanowalls as evident by the broken fibers in nearly straight-line patterns (Figure 2a), thus, minimizing random lateral buckling of the 1D structure.

To support our hypothesis, we carried out finite-element simulation to better understand the formation of the nanofibers in association with the buckling behavior. We simulated structures with AR = 2, 4, and 6, as a direct comparison to the experimental results shown in Figure 1. The simulation results show coinciding relationship between the AR and the buckling magnitude (**Figure 3**a–c). In the plots, the undulation

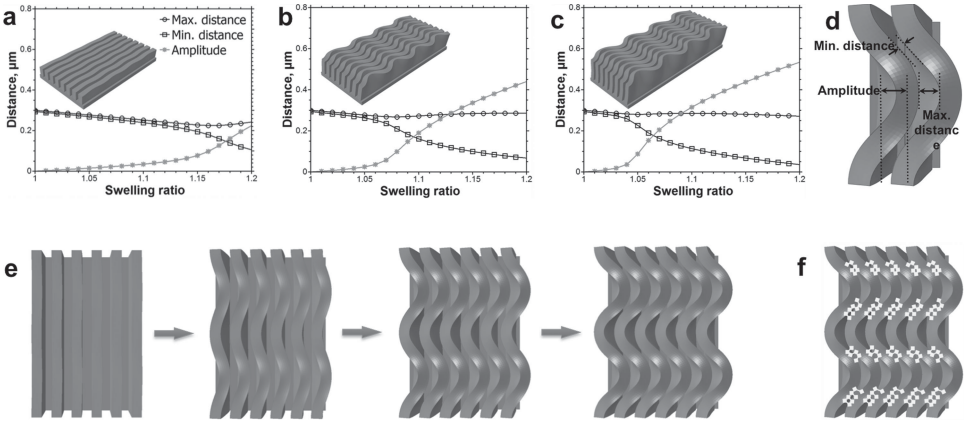

Figure 3. Finite-element simulation of the buckling behaviors of 1D nanowalls. a–c) Changes in the maximum distance (m), minimum distance between walls (o), and the undulation amplitude (★) of the same wall width (300 nm) but different aspect ratios, a) AR = 2, b) AR = 4, c) AR = 6 as a function of the swelling ratio. d) The corresponding 3D images of the predicted buckling behaviors of 1D walls of different aspect ratios with swelling ratio of 1.1. e) Top-view simulated images of the wall distance evolution during buckling. f) Illustration of nanofibers (white diamonds) formed mainly in the regions where wall distances are smaller than 200 nm.

amplitude increases as the swelling ratio increases. It also shows that the amplitude increases faster when AR is higher. The post-buckling shapes with swelling ratio 1.1 were shown in Figure 3d, which also matches the measured amplitudes well.

Finite-element analyses indeed provide more insights on the formation of nanofibers. As seen in Figure 1c, 2b, the distance between nanowalls, which was initially identical along the wall before buckling, varied as the buckling occurred. There are two causes that make the wall distance to be different in buckled configuration. Because the bottom of the 1D walls is constrained on the substrate, the 1D walls are not only buckled in the longitudinal direction but also twisted with out-of-plane displacement (see Supporting Information with Figure S4 for more details). Hence, the crest region has the maximum wall distance, and the middle point between two adjacent crest points has the minimum wall distance after buckling (see schematic in Figure 3d). The experimental results matched well with the simulations. At the swelling ratio 1.1, the wall distance appears to be larger than 250 nm along the entire structure. This relatively large gap between the walls gave only a few fiber formations as shown in Figure 1b. In the case of 300 nm width and AR = 6 (Figure 3c), however, the minimum wall distance is only about 120 nm at swelling ratio 1.1, while the maximum distance is around 280 nm. In the experiment, the nanofibers were mainly observed in the middle region between two adjacent crest points, of which wall distance was smaller than 200 nm (Figure 1c). A top-view of the wall distance evolution during buckling, as well as the nanofiber distribution can be found in Figure 3e,f. While it is possible that nanofibers could be formed by breaking the overlapping, weakly polymerized areas between nanowalls during buckling process, the above results (both experiments and simulation) clearly demonstrated that the buckling of 1D walls modulated the distance between the neighboring walls and the nanofibers were formed only where the distance between the walls was close enough due to the combination of higher exposure dosage and swelling during the lithographic process. We also simulated the exposure time effect to the gap size between nanowalls and thus nanofiber formation (see details in Figure S5 and related discussion in the Supporting Information).

As we mentioned earlier, more fibers were generated in the longer exposure sample as a result of decreased gap size because the higher AR should give larger amplitude of buckling. Upon drying, the buckled walls have a tendency to deswell and return to the original straight line geometry, and the distance between neighboring walls increase. However, with large quantities of fibers connecting the neighboring walls, the walls have to overcome the constraint imposed by the connected fibers to return to their original straight alignment when the walls deswell. Thus, we speculate that the nanofibers could help to maintain the order or registry of the buckled film and stabilize the long-range ordered nanowaves. To confirm this, we conducted experiments to remove the fibers, followed by re-swelling in PGMEA. A closer look of these fibers is shown in **Figure 4**a, a cross-sectional SEM image cut by focused ion beam (FIB). The nanofibers appeared throughout the sample from top to bottom. We took a buckled sample with many fibers (AR = 6), and covered half of it with aluminum foil while leaving the other half exposed to oxygen plasma (OP) treatment. The SEM image after OP is shown in Figure 4b, where the nanofibers were nearly completely removed in the exposed region. After removal the aluminum foil, the whole sample was put in the developer, followed by rinsing and drying steps performed before. For the half that still had fibers, the buckled morphology remained the same as before (Figure 4c). However, for the other half where fibers were removed, buckling lost the long-range ordering (Figure 4d), which unquestionably supported the role of nanofibers in maintaining the long-range ordering of nanowaves. When there were no fibers connecting the neighboring walls, each wall would buckle and compete with the neighboring ones for buckling space. On the other hand, since the space between each wall is very limited in our system comparing to the buckling amplitude, there is not enough space for the walls to deform in a completely random manner.

Since both 1D nanowalls and its buckled 2D nanowaves are highly ordered with sub-micrometer periodicity, they should have distinct optical properties. First, we compared the transmittance of the straight nanowalls, nanowaves, and random deformed line pattern from 350–800 nm (**Figure 5**a) and their corresponding photos were taken under ambient lighting (Figure 5b–d). The 1D nanowalls showed bright, reflected color,

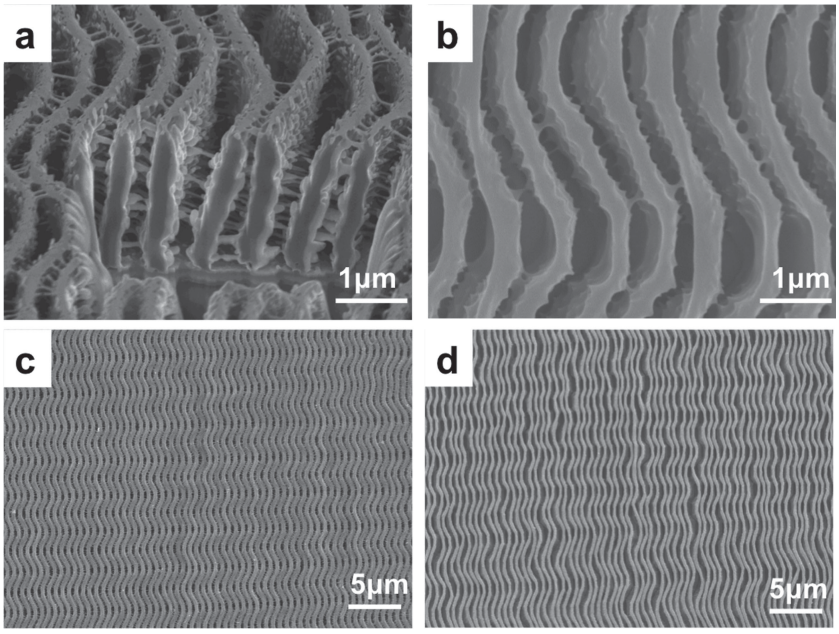

Figure 4. Effect of nanofibers in between nanowaves (AR = 6) to maintain the buckled structure during swelling. a) Cross-sectional SEM images of nanowaves with a large quantity of interconnecting nanofibers. b) Top-view SEM image of the nanowaves shown in (a) after 15 min oxygen plasma treatment, showing nearly no nanofibers left. c,d) Corresponding top-view SEM images of the nanowaves shown in (a,b) after re-swelling in PGMEA and drying.

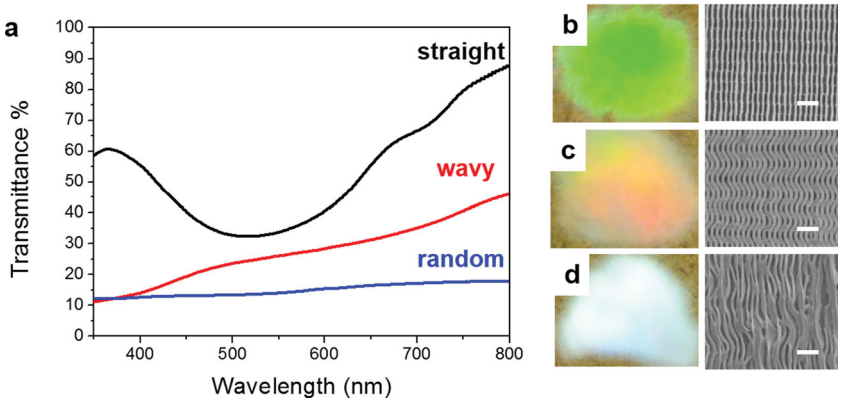

Figure 5. Comparison of the optical properties between straight 1D nanowalls, 2D nanowaves with long-range ordering, and randomly collapsed nanowaves. a) UV-Vis transmittance spectra. b–d) Photos and corresponding top-view SEM images of various nanostructures. Scale bar: 2 μm.

which was angle-dependent. Its transmittance spectrum dipped around 500–600 nm (near its periodic feature size), corresponding to the partial stop band of the 1D photonic structure. The sample with long-range ordered nanowaves also appeared colorful, although the reflectivity was not as strong as the straight nanowalls. Its transmittance was lower than that of the straight nanowall sample, and did not have the characteristic valley. As for the randomly deformed sample, it appeared white due to the random scattering from the film surface, thus, had the lowest transmittance among the three.

Lastly, we fabricated complex patterns using double exposure method for optical display. First, the SU-8 film was exposed to the interference beams to create the nanostructures, followed by UV exposure through a photomask with micrometer-sized patterns before PEB (see **Figure 6**a). After the development and CPD, the regions that were not double exposed would go through typical global buckling to form nanowaves, whereas the regions received double exposure would have higher crosslinking density and volume filling fraction, thus, forming straight nanowalls. As a proof-of-concept, we used two types of photomasks: one with 10 μm line width and 20 μm pitch, and the other with a character "N" in millimeter size. The sample double exposed from the 1D photomask showed alternating regions of nanowalls and nanowaves (Figure 6b,c) as expected. To better illustrate the color contrast in the nanowall and nanowave regions, we used a letter "N" photomask as shown in Figure 6d. The region within the character was double exposed and appeared more transparent than the surrounding regions, which appeared orange. The double exposed regions had higher volume filling fraction of SU-8 and the straight nanowalls were nearly connecting with each other. Therefore, they appeared more like a flat film, which was transparent. The color from the surrounding regions was the reflection color from the nanowaves.

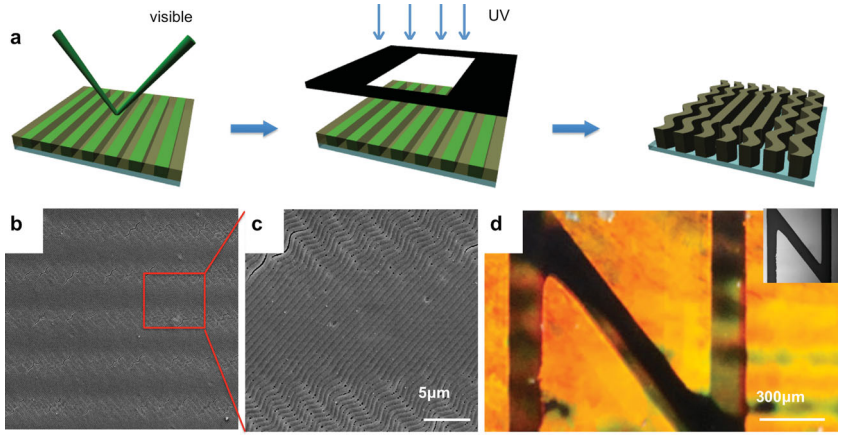

Figure 6. Double exposure patterning of nanowaves with nanowalls. a) Schematic illustration of the double exposure process, including HL at visible light first, followed by UV exposure through a photomask. b,c) SEM images of the hierarchical structure, consisting of nanowaves and nanowalls (width 300 nm, pitch 600 nm, AR ≈ 6) in a microscaled 1D grating (width10 μm, pitch 20 μm). c) Double exposed regions showing straight lines with higher filling fraction, while the single exposed regions showing typical nanowaves. d) Photo of a film double exposed with photomask of letter "N". Inset: optical image of the photomask. The double exposed region appeared more transparent than the surrounding due to higher filling fraction. The latter appeared orange due to reflection from the nanowaves.

3. Conclusions

In summary, we have fabricated long-range ordered 1D nanowalls and 2D nanowaves via HL and confined buckling. The extent of lateral undulation could be controlled by varying structure geometry and exposure dosage. Nanofibers were generated between the buckled nanowalls due to overlapping of the neighboring weakly crosslinked regions. By comparing experimental results with finite-element analysis, we investigated the buckling mechanism and confirmed that the nanofibers played a significant role that prevented deformed nanowalls from recovering to their original state, resulting in long-range ordered wavy structures. The ordered nanowave structure showed weaker reflecting color under an ambient light and lower transmittance compared to its straight counterpart, nanowalls; whereas the randomly deformed nanowaves appeared white. By combining HL and photolithography through a photomask, we demonstrated micropatterning of nanowaves vs. nanowalls for optical display. We believe that the investigation of buckling mechanism in 1D structures via nanofiber formation will provide new insights to fabricate highly ordered 2D and 3D structures by harnessing instability and pattern transformation. It will also allow us to create a rich library of complex patterns for advance applications, such as displays, waveguides, wire-grid linear polarizers, sensors, and substrates for guiding cell proliferation.

4. Experimental Section

Holographic Lithography: The 1D periodic nanowall pattern was fabricated by two-beam HL (see Figure 1a). In brief, the photoresist film was prepared from 40–58 wt% EPON SU-8 (Shell Chemical) and 2.0 wt% (relative to SU-8) Irgacure 261 (visible photoacid generator, Ciba Specialty Chemicals) in γ-butyrolactone (GBL, Sigma-Aldrich). The solution was spin coated on a pre-cleaned cover glass, followed by soft bake at 65 °C for 5 min and 95 °C for 15 min, respectively. The film was exposed to a diode-pumped Nd:YVO_4 laser (λ = 532 nm, Verdi-6, Coherent) with overall 1.0 W laser input (before beam splitting) for 15 to 20 s. The angle between two laser beams could be varied to achieve different feature size. After exposure, the film was post-exposure baked (PEB) at 65 °C and 95 °C for 2 min, respectively to crosslink the exposed regions, followed by development in propylene glycol monomethyl ether acetate (PGMEA, Sigma-Aldrich) for 30 min. Before drying in critical point dryer (CPD, SAMDRI-PVT-3D, tousimis), the wet samples were rinsed in isopropanol (IPA, Sigma-Aldrich) for 20 min.

Fiber Removal and Re-Swelling: A buckled sample with many connecting fibers (width of 300 nm, AR = 6) was half covered with aluminum foil and half exposed to oxygen plasma (30W, Harrick Plasma Cleaner PDC-001) for 15 min to remove the nanofibers. Then the aluminum foil was removed and the whole sample was developed in PGMEA for 1 h to re-swell the sample, followed by rinsing in IPA for 30 min, and critical point drying.

Double Exposure: The sample was first exposed to interference beam at 532 nm to create 1D nanowall pattern, followed by UV exposure (λ = 365 nm, 400 mJ cm^{-2}, 97435 Oriel Flood Exposure Source, Newport) through a photomask, including a line pattern with 10 μm width and 20 μm pitch, and a "N" letter pattern in millimeter. The film was then PEB, developed in PGMEA and CPD dried as described earlier.

Characterization: SEM images were taken from FEI Strata DB235 Focused Ion Beam (FIB) system and the cross-sectional images were taken from samples milled by the Gallium ion beam. The transmission spectra were acquired by UV-Vis spectrometer (Varian Cary 100).

Finite-Element Analysis:. ABAQUS/Standard,[32] a commercial finite-element analysis software, was used. Young's modulus and Poisson's ratio of SU-8 were chosen to be 1.7 GPa and 0.49 according to the experimental measurement. Nonlinear static analyses were performed for the post-buckling prediction based on the buckling analysis. Three-dimensional continuum element (C3D8) was adopted with 50 nm in characteristic element length. The swelling ratio of SU-8 was assumed to vary from 1.0 to 1.2 throughout the analyses. More detailed finite-element mesh design and boundary conditions are available in the Supporting Information.

Supporting Information

Supporting Information is available from the Wiley Online Library or from the author.

Acknowledgements

The research was supported by the National Science Foundation (NSF), grant #CMMI-0900468 and EFRI-1038215. Penn Regional Nanotech facility (PRFN) is acknowledged for accessing SEM. Y.C. and I.C. acknowledge support from the KIST Global Research Program (grant #2Z03770) funded by Korea Institute of Science and Technology. Y.C. also acknowledges support from the Research Fellowship for Young Scientists Program of KRCF.

Received: August 12, 2013
Revised: October 15, 2013
Published online: December 16, 2013

[1] J. D. Joannopoulos, S. G. Johnson, J. N. Winn, R. D. Meade, In *Photonic Crystals*, 2nd ed., Princeton University Press, Princeton, **2008**.
[2] T. Gorishnyy, C. K. Ullal, M. Maldovan, G. Fytas, E. L. Thomas, *Phys. Rev. Lett.* **2005**, *94*, 4.
[3] T. N. Krupenkin, J. A. Taylor, T. M. Schneider, S. Yang, *Langmuir* **2004**, *20*, 3824–3827.
[4] M. K. Kwak, H. E. Jeong, T. I. Kim, H. Yoon, K. Y. Suh, *Soft Matter* **2010**, *6*, 1849–1857.
[5] H. E. Jeong, K. Y. Suh, *Nano Today* **2009**, *4*, 335–346.
[6] M. K. Kwak, C. Pang, H.-E. Jeong, H.-N. Kim, H. Yoon, H.-S. Jung, K.-Y. Suh, *Adv. Funct. Mater.* **2011**, *21*, 3606–3616.
[7] C. S. Chen, J. Tan, J. Tien, *Annu. Rev. Biomed. Eng.* **2004**, *6*, 275–302.
[8] Y. C. Tseng, A. U. Mane, J. W. Elam, S. B. Darling, *Adv. Mater.* **2012**, *24*, 2608–2613.
[9] M. K. Hooda, M. Wadhwa, S. Verma, M. M. Nayak, P. J. George, A. K. Paul, *Vacuum* **2010**, *84*, 1142–1148.
[10] M. Ahn, R. K. Heilmann, M. L. Schattenburg, *J. Vac. Sci. Technol. B* **2007**, *25*, 2593–2597.
[11] K. Hosomi, T. Fukamachi, H. Yamada, T. Katsuyama, Y. Arakawa, *Photonics Nanostruct.* **2006**, *4*, 30–34.
[12] T. Tanaka, M. Morigami, N. Atoda, *Jpn. J. Appl. Phys.* **1993**, *32*, 6059–6064.
[13] M. P. Stoykovich, H. B. Cao, K. Yoshimoto, L. E. Ocola, P. F. Nealey, *Adv. Mater.* **2003**, *15*, 1180–1184.
[14] D. Chandra, S. Yang, *Langmuir* **2009**, *25*, 10430–10434.
[15] D. Chandra, S. Yang, *Acc. Chem. Res.* **2010**, *43*, 1080–1091.
[16] S. J. DuPont, R. S. Cates, P. G. Stroot, R. Toomey, *Soft Matter* **2010**, *6*, 3876–3882.
[17] M. K. Kang, R. Huang, *Int. J. Appl. Mech.* **2011**, *3*, 219–233.
[18] M. Darnon, T. Chevolleau, O. Joubert, S. Maitrejean, J. C. Barbe, J. Torres, *Appl. Phys. Lett.* **2007**, *91*, 194103.
[19] H. Yoon, A. Ghosh, J. Y. Han, S. H. Sung, W. B. Lee, K. Char, *Adv. Funct. Mater.* **2012**, *22*, 3723–3728.
[20] J. H. Moon, J. Ford, S. Yang, *Polym. Adv. Tech.* **2006**, *17*, 83–93.
[21] J. H. Moon, S. Yang, *Chem. Rev.* **2010**, *110*, 547–574.
[22] X. Zhu, G. Liang, Y. Xu, S.-C. Cheng, S. Yang, *J. Opt. Soc. Am. B* **2010**, *27*, 2534–2541.
[23] J. M. Shaw, J. D. Gelorme, N. C. LaBianca, W. E. Conley, S. J. Holmes, *IBM J. Res. Dev.* **1997**, *41*, 81–94.
[24] M. Campbell, D. N. Sharp, M. T. Harrison, R. G. Denning, A. J. Turberfield, *Nature* **2000**, *404*, 53–56.
[25] Z. Zhou, Q.-A. Huang, W. Li, W. Lu, Z. Zhu, M. Feng, In The Swelling Effects During the Development Processes of Deep UV Lithography of SU-8 Photoresists: Theoretical Study, Simulation and Verification, Sensors, 2007 IEEE, Atlanta, Georgia, 28–31 Oct. 2007; 2007; pp 325–328.
[26] K. Wouters, R. Puers, *J. Micromech. Microeng.* **2010**, *20*, 095013.
[27] S. Singamaneni, K. Bertoldi, S. Chang, J. H. Jang, S. L. Young, E. L. Thomas, M. C. Boyce, V. V. Tsukruk, *Adv. Funct. Mater.* **2009**, *19*, 1426–1436.
[28] S. Singamaneni, K. Bertoldi, S. Chang, J. H. Jang, E. L. Thomas, M. C. Boyce, V. V. Tsukruk, *ACS Appl. Mater. Interfaces* **2009**, *1*, 42–47.
[29] J. H. Jang, C. Y. Koh, K. Bertoldi, M. C. Boyce, E. L. Thomas, *Nano Lett.* **2009**, *9*, 2113–2119.
[30] H. N. Kim, J. H. Kang, W. M. Jin, J. H. Moon, *Soft Matter* **2011**, *7*, 2989–2993.
[31] S. H. Park, T. W. Lim, D. Y. Yang, N. C. Cho, K. S. Lee, *Appl. Phys. Lett.* **2006**, *89*, 173133.
[32] H. D. Hibbitt, *Nucl. Eng. Des.* **1984**, *77*, 271–297.